

Investigation of fibre-optic cable formation in DAS acquisition

Heather K. Hardeman-Vooy* and Michael P. Lamoureux *

ABSTRACT

In this paper, we provide insight into the amplitude response of a distributed acoustic sensor. Using techniques from algebraic topology, we know that there is a mathematical foundation for deforming a helically wound fibre into a straight fibre for a DAS system. We model what occurs as a helically wound fibre deforms into a straight fibre optic cable. The deformation allows us to consider how the strain tensor is affected by studying its determinant, trace, and eigenvalues.

INTRODUCTION

The flexibility of fibre-optic cables provides more benefits than simply sensitivity to strain. In fact, this flexibility allows it to be bent into many different formations in order to increase its sensitivity to strain. A fibre structure of particular interest is the helically wound fibre. Figure 1 provides an example of a helically wound fibre-optic cable. One

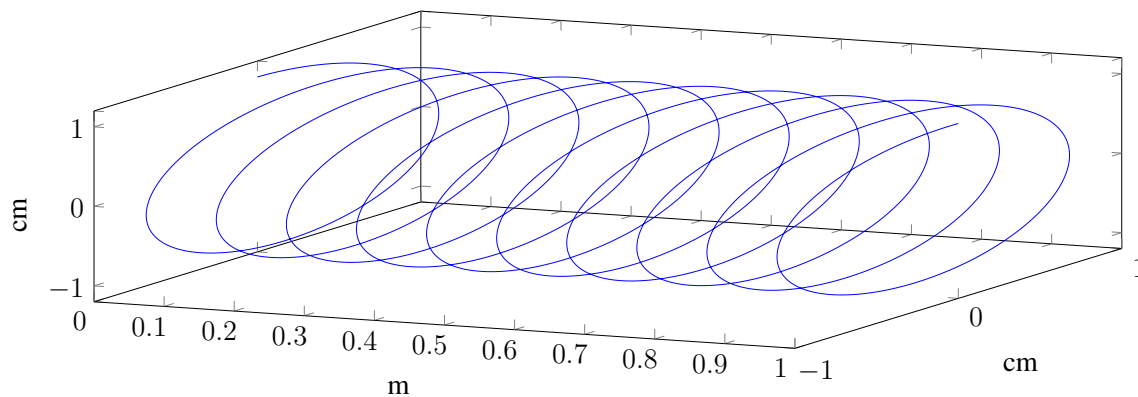


FIG. 1: An example of a helically wound fibre-optic cable in a DAS sensor.

issue of the straight fibre is that it cannot detect the wave when it hits the straight fibre perpendicularly. Orienting the fibre helically provides a way for the fibre to detect waves oriented perpendicular to the straight fibre.

In theory, the helically wound fibre should provide more information about the area around the fibre. However, in practice, it appears the helical fibre produces a much lower signal than the straight fibre. There are many questions as to why the helically wound fibre does not appear to perform as well as the straight fibre in real world applications. A considerable amount of investigation has gone into this question, even within CREWES. In this paper, we attempt to offer mathematical insight into the differences between the signals in the straight and helically wound fibre.

In this paper, we produce bounds for the amplitude response of the fibre for various

*University of Calgary, Department of Mathematics

configuration whether a gauge length is applied or not. Afterwards, we explain how the amplitude response of the helical fibre is connected via a homotopy to the amplitude response of the straight fibre. Employing this fact, we model DAS data to compare the helically wound fibre and the straight fibre. The example compares the results of a 2.54cm radius helical fibre laid horizontally along the earth's surface deforming into the straight fibre.

We find the bounds for the amplitude $A(s, t)$ of the data to be

$$\Lambda_{\min} \leq A(s, t) \leq \Lambda_{\max}, \quad (1)$$

where Λ_{\min} is the minimum eigenvalue for all eigenvalues λ_{\min} for the strain matrix $\epsilon(\mathbf{p}(s), t)$ and Λ_{\max} is the maximum eigenvalue for all eigenvalues λ_{\max} for the strain matrix $\epsilon(\mathbf{p}(s), t)$. The bounds for the amplitude $(A * g)(s, t)$ of the data with the gauge length applied is

$$\gamma \Lambda_{\min} \leq (A * g)(s, t) \leq \gamma \Lambda_{\max} \quad (2)$$

where γ is the distance of the gauge length and g is the gauge length function

$$g(\tau) = \begin{cases} 1 & -\frac{\gamma}{2} \leq \tau \leq \frac{\gamma}{2}; \\ 0 & \text{otherwise.} \end{cases} \quad (3)$$

We also show that a homotopy exists between the amplitude response of the helically wound fibre and the amplitude response of the straight fibre. This means that the helically wound fibre can be deformed into the straight fibre. The homotopy allows us to compare the responses of the straight and helical fibre.

We use the homotopy to model helical fibre in two examples. The first example shows the results of a 2.54cm radius helix fibre, laid horizontally along the ground, deforming into the straight fibre. We consider the result at four locations and see that the L^2 -norm of the data when the gauge length is applied increases across the homotopy from the helical fibre to the straight fibre; however, the norms of the data, without the gauge length applied, as well as the traces, determinants, and eigenvalues of the strain matrices decreases from the helical fibre to the straight fibre across the homotopy.

BOUNDS ON THE AMPLITUDE OF DAS DATA

In Hardeman-Vooy's and Lamoureux (2018), we saw several examples where the helically wound fibre produced an amplitude response which was significantly smaller than the amplitude response of the straight fibre. The question arises as to whether this holds for all helical fibre or just the examples we saw in Hardeman-Vooy's and Lamoureux (2018). Instead of using brute force to answer this question, we provide bounds on the amplitude, $A(s, t)$, and the amplitude of the data when a gauge length is applied, $(A * g)(s, t)$ using the model described in Hardeman-Vooy's and Lamoureux (2018). These bounds provide us with the minimum and maximum amplitude for any choice of helical radius and number of rotations per meter.

Recall in the model that the amplitude response of a distributed acoustic sensor is described using the following equation:

$$A(s, t) = \mathbf{T}_p^\top(s) \epsilon(\mathbf{p}(s), t) \mathbf{T}_p(s), \quad (4)$$

where the matrix $\epsilon(\mathbf{p}(s), t)$ is the strain at the point s on the path \mathbf{p} of the fibre at time t . The vector $\mathbf{T}_{\mathbf{p}}(s)$ is the unit tangent path of the fibre at s .

In order to find these amplitude bounds, we need to use some results from linear algebra. We start by considering some definitions.

Definition 1. Let A be a $d \times d$ symmetric matrix. The matrix A is called *positive semi-definite* if all its eigenvalues are non-negative. This is denoted as $A \succeq 0$, where 0 denotes the $d \times d$ zero matrix. A positive definite matrix A satisfies the condition

$$A \succ 0 \iff x^\top Ax \geq 0 \quad \forall x \in \mathbb{R}^d. \quad (5)$$

We also need the following ordering for matrices.

Definition 2. For any two symmetric matrices A and B , the *Löwner ordering*, or *postive semi-definite ordering*, is defined as $A \succeq B$ if $A - B \succeq 0$.

Now we are prepared to prove the following lemmas in order to find bounds for the amplitude response of the fibre.

Lemma 3. Let A be a symmetric matrix. Let λ_{\min} and λ_{\max} respectively denote the smallest and largest eigenvalues of A . Then

$$\lambda_{\min} \cdot I \preceq A \preceq \lambda_{\max} I. \quad (6)$$

The strain tensor ϵ is symmetric; hence via application of Lemma 3, ϵ is bounded by,

$$\lambda_{\min} \cdot I \preceq \epsilon \preceq \lambda_{\max} \cdot I, \quad (7)$$

in the Lö order. We also get the following lemma from linear algebra.

Lemma 4. For symmetric A and B , $A \succeq B$ if and only if $v^\top Av \geq v^\top Bv$ for all vectors v .

Since we know that Equation 7 holds, by Lemma 4,

$$\mathbf{T}_{\mathbf{p}}^\top \lambda_{\min} \cdot I \mathbf{T}_{\mathbf{p}} \leq \mathbf{T}_{\mathbf{p}}^\top \epsilon \mathbf{T}_{\mathbf{p}} \leq \mathbf{T}_{\mathbf{p}}^\top \lambda_{\max} \cdot I \mathbf{T}_{\mathbf{p}} \quad (8)$$

$$\implies \mathbf{T}_{\mathbf{p}}^\top \lambda_{\min} \cdot I \mathbf{T}_{\mathbf{p}} \leq A(s, t) \leq \mathbf{T}_{\mathbf{p}}^\top \lambda_{\max} \cdot I \mathbf{T}_{\mathbf{p}} \quad (9)$$

$$\implies \lambda_{\min} \|\mathbf{T}_{\mathbf{p}}\|_2^2 \leq A(s, t) \leq \lambda_{\max} \|\mathbf{T}_{\mathbf{p}}\|_2^2. \quad (10)$$

Recall that since $\mathbf{T}_{\mathbf{p}}$ is the unit tangent path of the fibre, $\|\mathbf{T}_{\mathbf{p}}\|_2^2 = 1$. Hence, the bounds for the amplitude $A(s, t)$ will be

$$\lambda_{\min}(s, t) \leq A(s, t) \leq \lambda_{\max}(s, t). \quad (11)$$

The eigenvalues $\lambda_{\min}(s, t)$ and $\lambda_{\max}(s, t)$ are the minimum and maximum eigenvalues of the strain matrix $\epsilon(\mathbf{p}(s), t)$ at the point (s, t) on the fibre path \mathbf{p} , respectively. Let

$$\Lambda_{\min} = \min_{\substack{s \in \mathbb{R}; \\ t \in [0, \infty)}} \lambda_{\min}(s, t) \quad (12)$$

and

$$\Lambda_{\max} = \max_{\substack{s \in \mathbb{R}; \\ t \in [0, \infty)}} \lambda_{\max}(s, t). \quad (13)$$

We then have

$$\Lambda_{\min} \leq \lambda_{\min} \leq A(s, t) \leq \lambda_{\max} \leq \Lambda_{\max}, \quad (14)$$

from whence we derive

$$\Lambda_{\min} \leq A(s, t) \leq \Lambda_{\max}. \quad (15)$$

When applying the gauge length to the waveform response, we convolve the amplitude of the waveform $A(s, t)$ with the gauge length function

$$g(\tau) = \begin{cases} 1 & -\frac{\gamma}{2} \leq \tau \leq \frac{\gamma}{2}; \\ 0 & \text{otherwise,} \end{cases} \quad (16)$$

where γ is the distance of gauge length. We calculate the data with the gauge length applied via the convolution

$$(A * g)(s, t) = \int_{-\infty}^{\infty} A(\tau, t)g(s - \tau)d\tau \quad (17)$$

$$= \int_{s-\frac{\gamma}{2}}^{s+\frac{\gamma}{2}} A(\tau, t)d\tau. \quad (18)$$

Recall from calculus that the following inequality holds for integrals:

Lemma 5. *If $m \leq f(x) \leq M$ for $a \leq x \leq b$ then*

$$m(b - a) \leq \int_a^b f(x)dx \leq M(b - a). \quad (19)$$

Using Lemma 5, we then find that the data with the gauge length applied $A_G(s, t)$ is bounded between

$$\int_{s-\frac{\gamma}{2}}^{s+\frac{\gamma}{2}} \Lambda_{\min}d\tau \leq \int_{s-\frac{\gamma}{2}}^{s+\frac{\gamma}{2}} A(\tau, t)d\tau \leq \int_{s-\frac{\gamma}{2}}^{s+\frac{\gamma}{2}} \Lambda_{\max}d\tau \quad (20)$$

$$\implies \Lambda_{\min} \int_{s-\frac{\gamma}{2}}^{s+\frac{\gamma}{2}} d\tau \leq (A * g)(s, t) \leq \Lambda_{\max} \int_{s-\frac{\gamma}{2}}^{s+\frac{\gamma}{2}} d\tau \quad (21)$$

$$\implies \Lambda_{\min} \left(s + \frac{\gamma}{2} - \left(s - \frac{\gamma}{2} \right) \right) \leq (A * g)(s, t) \leq \Lambda_{\max} \left(s + \frac{\gamma}{2} - \left(s - \frac{\gamma}{2} \right) \right) \quad (22)$$

$$\implies \gamma \Lambda_{\min} \leq (A * g)(s, t) \leq \gamma \Lambda_{\max}. \quad (23)$$

With these arguments, we have produced bounds for the amplitude response of the data both when a gauge length is applied to the data, and when it is not applied to the data.

COMPARISON OF STRAIGHT AND HELICALLY WOUND FIBRE

One way to compare the straight and helically wound fibre directly is by using a homotopy.

Definition 6. Let X, Y be topological spaces, and $f, g : X \rightarrow Y$ continuous maps. A *homotopy* from f to g is a continuous function $F : X \times [0, 1] \rightarrow Y$ satisfying

$$F(x, 0) = f(x) \quad \text{and} \quad F(x, 1) = g(x), \quad (24)$$

for all $x \in X$. If a homotopy exists, we say that f is homotopic to g and write $f \simeq g$.

Figure 2 gives a visual idea of what the homotopy does with regards to the fibre-optic cable. As we move over the homotopy, the shape of the helix deforms along the black arrows in the figure to the straight fibre. In Figure 3, a 2π cross-section of a helical fibre with radius h_r is considered. For certain values of $w \in [0, 1]$, the radius of the helix shrinks. Figure 3 shows what occurs given four values of w : 0, w_1 , w_2 , and 1.

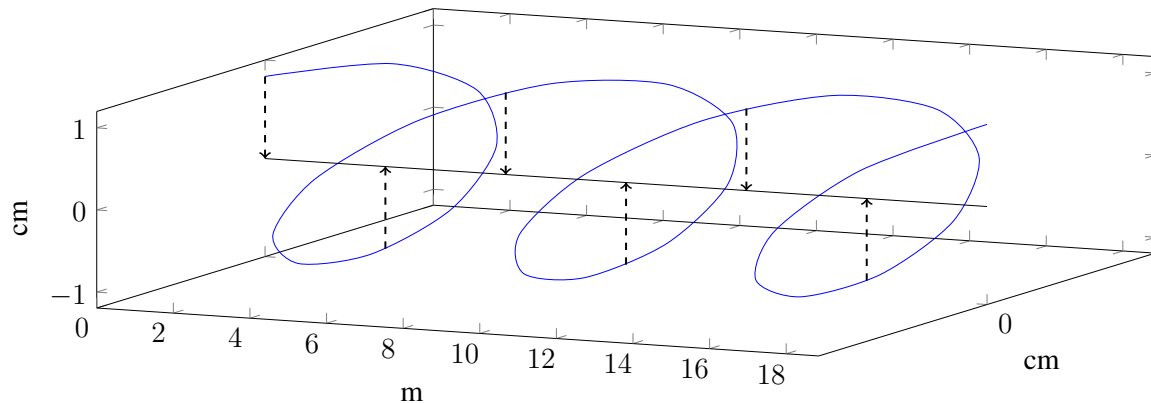


FIG. 2: A helix deforming to a straight line.

A homotopy describes how one shape can be deformed into another shape. Its existence suggests that we can deform the helically wound fibre-optic cable into a straight fibre-optic cable. It also allows us to compare two different matrices or in this case, data sets. We can compare what happens as the helically wound fibre slowly deforms into the straight fibre in a DAS system. We assume that the helical fibre holds its shape without any support. In reality, the helix would have the support of foam, aluminum, or some other material. We leave that to future work. In the next section, we use the homotopy to compare the two formations of fibre. We will specifically compare the norms of the data over the deformation in the following section.

Deformation model

With a homotopy between the amplitude response of the straight fibre and the amplitude response of the helical fibre, we create a model to study what occurs as the fibre deforms from helically wound to straight. In the following equations, we use MATLAB notation to

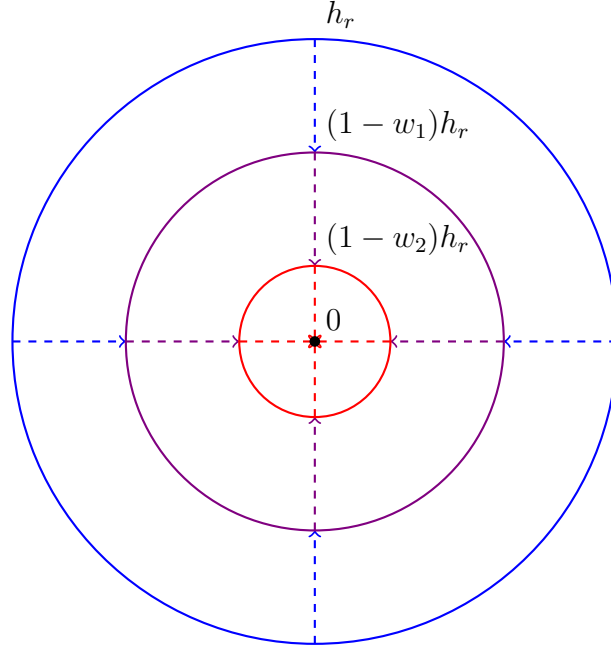


FIG. 3: A 2π cross-section of a fibre-optic cable with helical radius h_r deforming into a straight fibre over four choices of w in the homotopy: 0 (blue), w_1 (purple), w_2 (red), and 1 (black).

explain the model. Consider the following fibre configuration:

$$\mathbf{p}(s) = [s; 100 + h_r \cos(2\pi h_n s); -0.5 + h_r \sin(2\pi h_n s)] \quad (25)$$

where h_r is the helical radius and h_n is the number of rotations per meter. We find the equation for the straight fibre $\mathbf{p}_{\text{str}}(s)$ by setting the helical radius $h_r = 0$ and the number of rotations $h_n = 0$, which gives

$$\mathbf{p}_{\text{str}}(s) = [s; 100; -0.5] \quad (26)$$

and

$$\mathbf{p}_{\text{hel}}(s) = [s; 100 + h_r \cos(2\pi h_n s); -0.5 + h_r \sin(2\pi h_n s)] \quad (27)$$

where we choose $h_r = 2.54\text{cm}$ and $h_n = 10$ rotations. Therefore, the homotopy F becomes

$$F(s, w) = (1 - w)\mathbf{p}_{\text{hel}}(s) + w\mathbf{p}_{\text{str}}(s) \quad (28)$$

$$= (1 - w)[s; 100 + h_r \cos(2\pi h_n s); -0.5 + h_r \sin(2\pi h_n s)] + w[s; 100; -0.5] \quad (29)$$

$$= [(1 - w)s + ws; (1 - w)(100 + h_r \cos(2\pi h_n s)) + w100; (1 - w)(-0.5 + h_r \sin(2\pi h_n s)) + w(-0.5)] \quad (30)$$

$$= [s; 100 + (1 - w)h_r \cos(2\pi h_n s); -0.5 + (1 - w)h_r \sin(2\pi h_n s)]. \quad (31)$$

The w from the homotopy only affects the sine and cosine from the helical fibre. This follows geometrically given that the homotopy deforms a helix into a straight line.

We use $F(s, w)$ to represent the fibre path in our model. The values of w vary in order to show how $A(s, t)$ deforms over w from the helical $A_{\text{hel}}(s, t)$ to the straight $A_{\text{str}}(s, t)$. Specifically, we choose

$$w \in \left\{ 0, \frac{1}{7}, \frac{1}{4}, \frac{1}{2}, \frac{3}{5}, \frac{3}{4}, 1 \right\}. \quad (32)$$

To give examples outside multiples of $1/4$, we pick values of $w = 1/7$ and $w = 3/5$. We position the source at four different locations on the fibre to study how the position of the source affects the response of the fibre. We choose the following four locations with respect to the fibre in our model:

1. Location 1 - [101,105,0];
2. Location 2 - [106,105,0];
3. Location 3 - [111,105,0];
4. Location 4 - [100,111,0].

Let us begin by considering the results for all w when the source is at Location 1. Figures 4 – 7 show the fibre deforming from helical fibre of radius 2.54cm for 10 rotations per meter of fibre to straight fibre. We plug the different values of w into the homotopy F from Equation 31 and use it for the path of the fibre. The left column of each set of figures shows the data without the gauge length applied and the right column depicts the data with the 10 meter gauge length applied.

Figure 4 shows the 2.54cm helical fibre at the top and the 2.54cm radius diminished by $1/7$ th of the radius on the bottom row. The data without the gauge length applied as seen on the left shows some evidence of the helical fibre given the presence of oscillations in the signal, whereas the version of the data with the gauge length applied on the right does not have these oscillations. At least for this size of helix and gauge length, the gauge length causes the parts of the data which highlight the helix to disappear. Moreover, the signal of the data with the gauge length applied looks brighter and larger because the gauged data applies a sampling rate of $\Delta x = 2/3\text{m}$ which is typical for real data. The data without a gauge length applied has a sampling rate of $\Delta x = 1/3\text{m}$ because we need at least three points per rotation in order to realize the helix.

In Figure 5, the helical shape of the fibre becomes much more prominent in the data without a gauge length applied on the left as the radius decreases; however, applying the gauge length causes the helix to disappear from the data. The prominence of the helix may be due to the number of sample points employed to create the helical data set. The smaller helix benefits from the fewer sample points, while the larger helix did not. It may also be due to how close the source is to the fibre.

Focusing now on the data with the 10 meter gauge length applied, notice that the helical fibre of radius 2.54cm decreased by $1/4$ of the radius (top right) does not have distinguishable S-wave response, but decreasing the radius by half of the radius (bottom right) produces a visible S-wave.

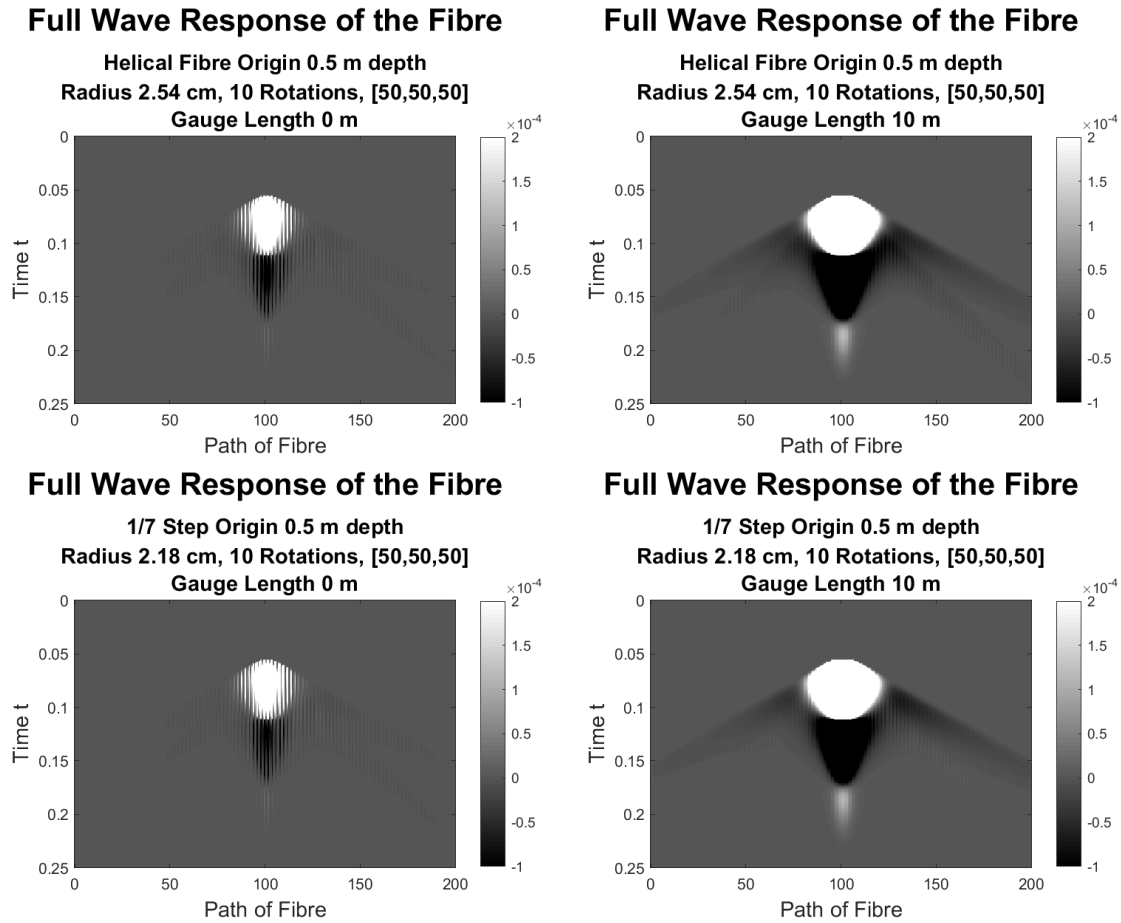


FIG. 4: (Left column) The data without the gauge length applied (top) helical fibre and (bottom) helical fibre diminished by 1/7-th of the radius when the source is at Location 1. (Right column) The 10 m gauge length applied to data seen in the left column.

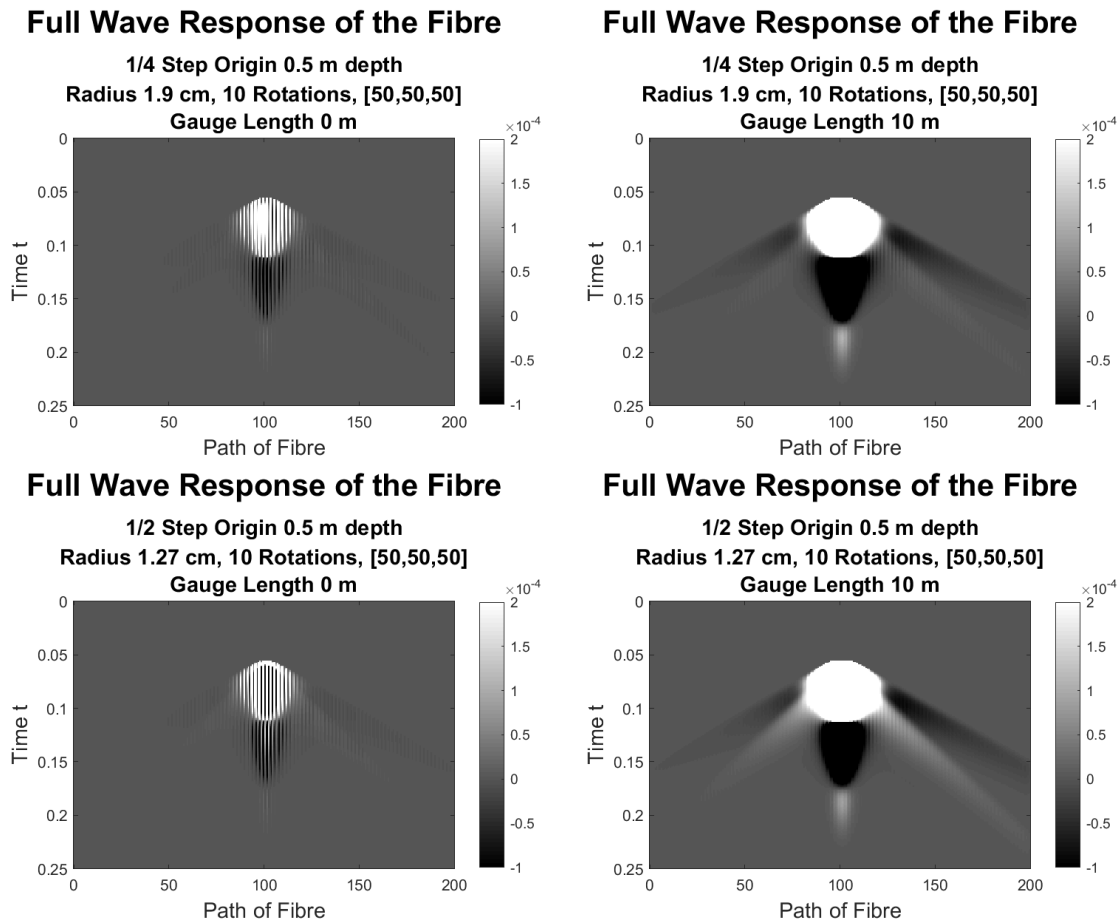


FIG. 5: (Left column) The data without the gauge length applied (top) helical fibre diminished by 1/4-th of the radius and (bottom) helical fibre diminished by 1/2-th of the radius when the source is at Location 1. (Right column) The 10m gauge length applied to data seen in the left column.

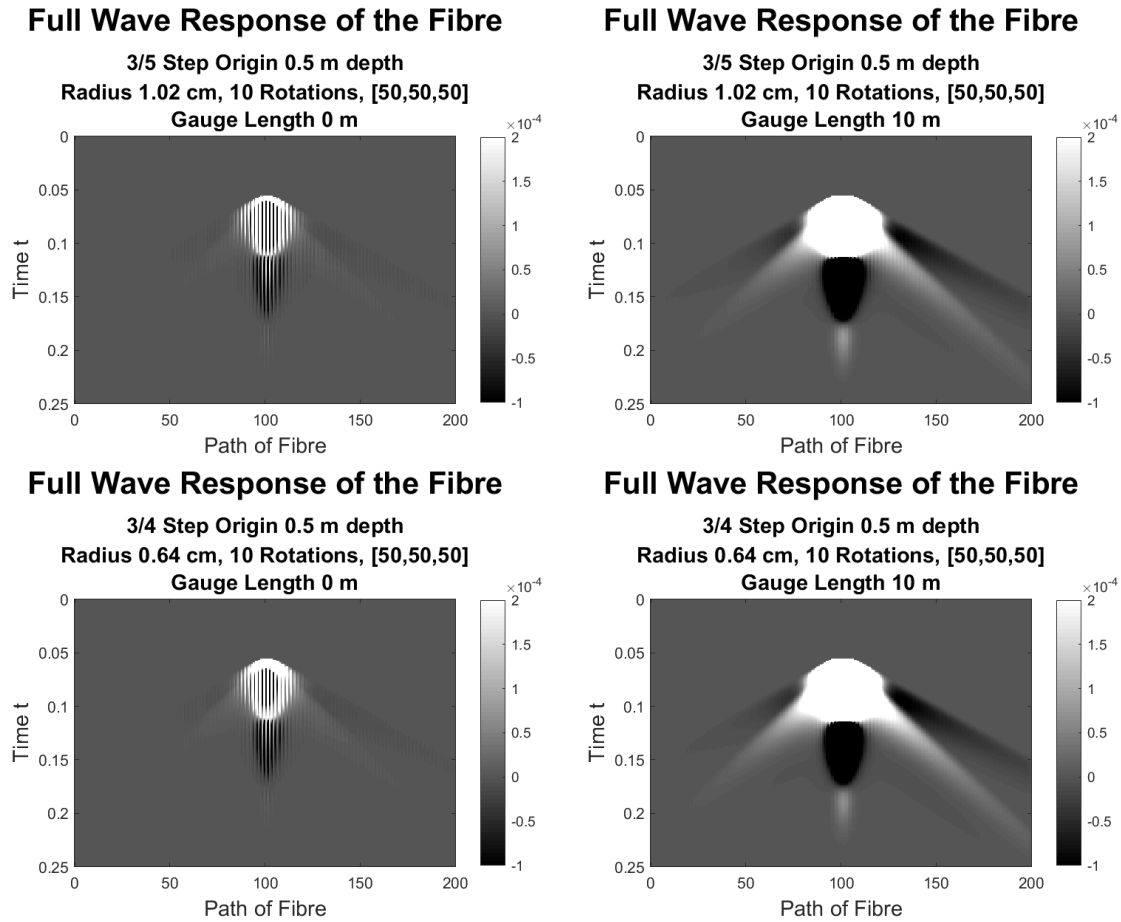


FIG. 6: (Left column) The data without the gauge length applied (top) helical fibre diminished by $3/5$ -th of the radius and (bottom) helical fibre diminished by $3/4$ -th of the radius when the source is at Location 1. (Right column) The 10m gauge length applied to data seen in the left column.

Interestingly, Figure 6 provides even more evidence of the S-wave response as the radius of the helix decreases. The helix can still be distinguished in the data without the gauge length applied on the left; however, it does not appear in the data with a gauge length applied on the right, which is to be expected given the results found in Figure 4 and 5.

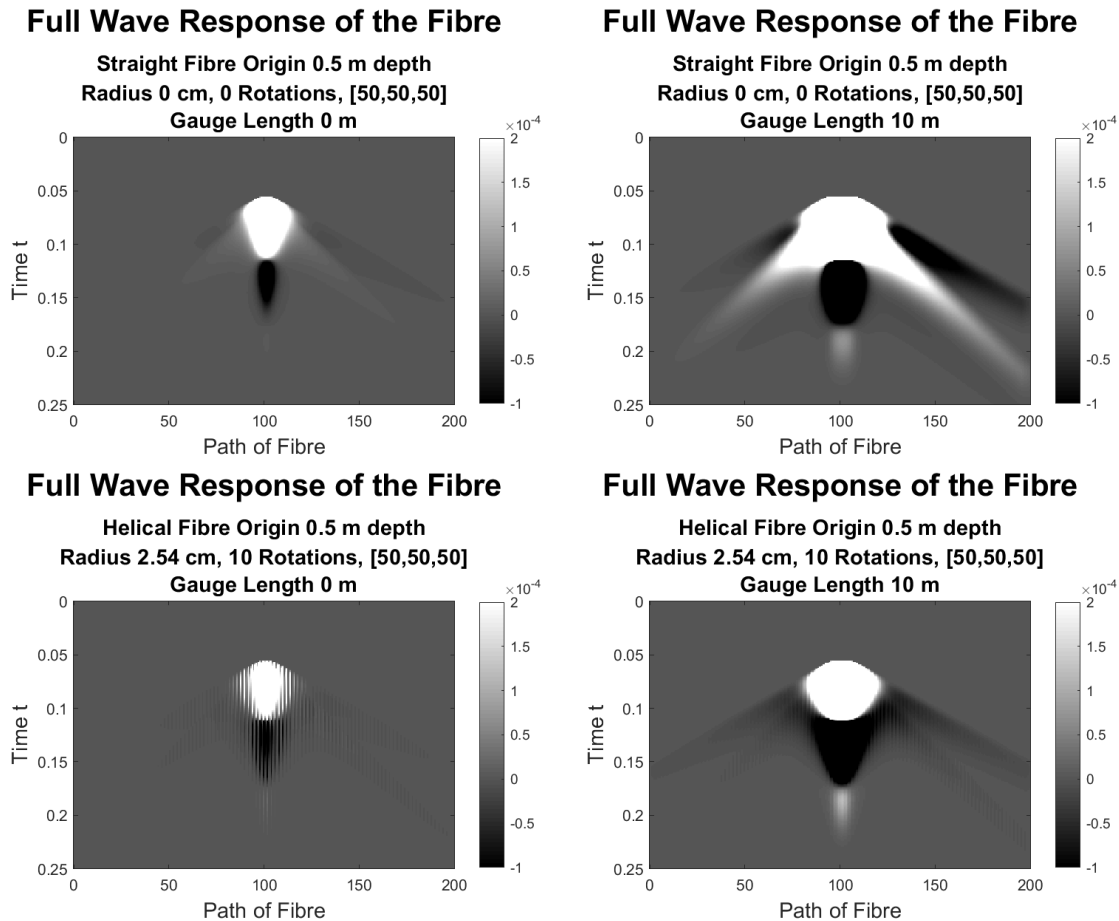


FIG. 7: (Left column) The data without the gauge length applied (top) straight fibre and (bottom) helical fibre at Location 1. (Right column) The 10m gauge length applied to data seen in the left column at Location 1.

Figure 7 shows this pattern continuing. We compare the final results of the homotopy by including the results from the helical fibre in the bottom row of Figure 7. The S-wave is present for the straight fibre whereas it is not evident for the helical fibre of radius 2.54cm. the signal from the straight fibre possesses a flatter peak than the helical fibre. The tail of the signal for the straight fibre is wider. While the signal of the helical fibre is smaller than the signal of the straight fibre, it appears to be more precise with regards to the shape of the hyperbola; however, it is much more difficult to distinguish the S-wave response in the helical fibre response than it is in the straight fibre response. Recall from Hardeman-Vooy's and Lamoureux (2018) that the helical fibre's S-wave response had a smaller amplitude than the straight fibre's S-wave response. the amplitude of the helical fibre's S-wave response is present.

Figure 8 depicts the results of the straight fibre (top) and the helical fibre (bottom) when

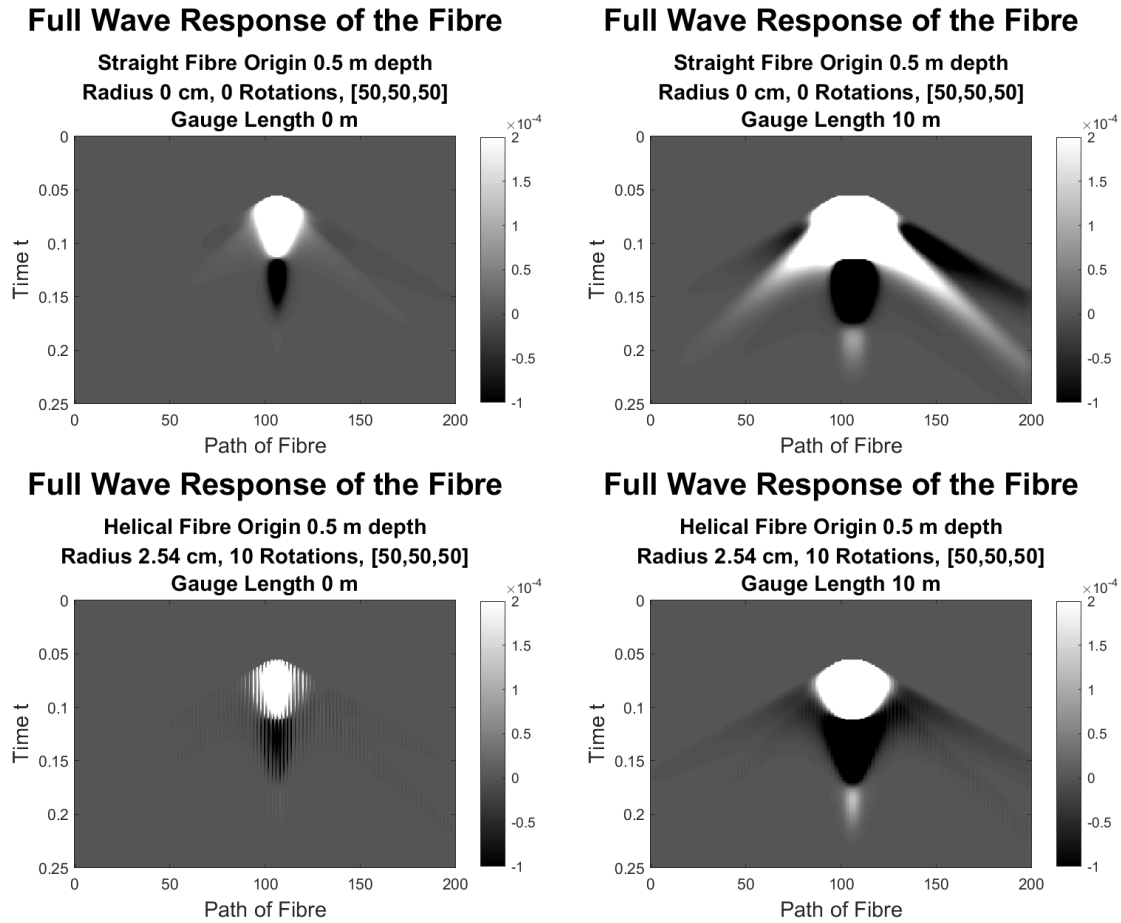


FIG. 8: (Left column) The data without the gauge length applied (top) straight fibre and (bottom) helical fibre at Location 2. (Right column) The 10m gauge length applied to data seen in the left column at Location 2.

the source is at Location 2. The hyperbola is to right of where it was in the data for Location 1. Applying the gauge length to the data (right) has similar results to the data at Location 1. The peak of the straight fibre's response is flattened. The helical fibre's response no longer has evidence of a helix once the gauge length is applied.

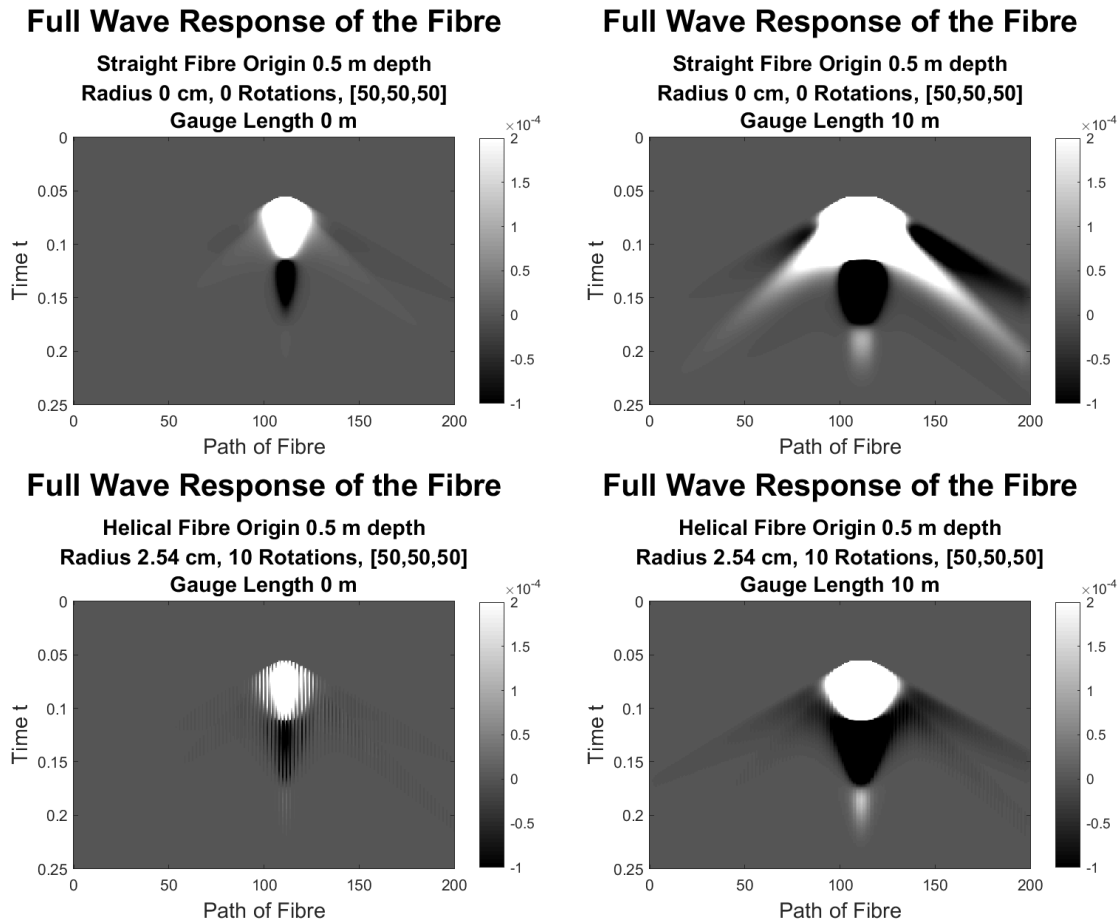


FIG. 9: (Left column) The data without the gauge length applied (top) straight fibre and (bottom) helical fibre at Location 3. (Right column) The 10m gauge length applied to data seen in the left column at Location 3.

In Figure 9, the results for the data at Location 3 produce a similar outcome to the previous two locations. The hyperbola response has once again moved toward the right. This is because Location 3 occurs at 111 meters down the length of the fibre.

Figure 10 presents the results for Location 4. Recall that Location 4 is near the center of the fibre but 11 meters away from the fibre formation, unlike the previous three locations which were 5 meters away from the fibre. The amplitude response of both the helical and straight fibre is much smaller for the new location, both when the gauge length is applied to the data and when it is not, than for the previous four locations. Once again when we apply the gauge length to the straight and helical fibre, it is difficult to distinguish the S-wave response in the helical fibre, while we can locate it in the straight fibre's response.

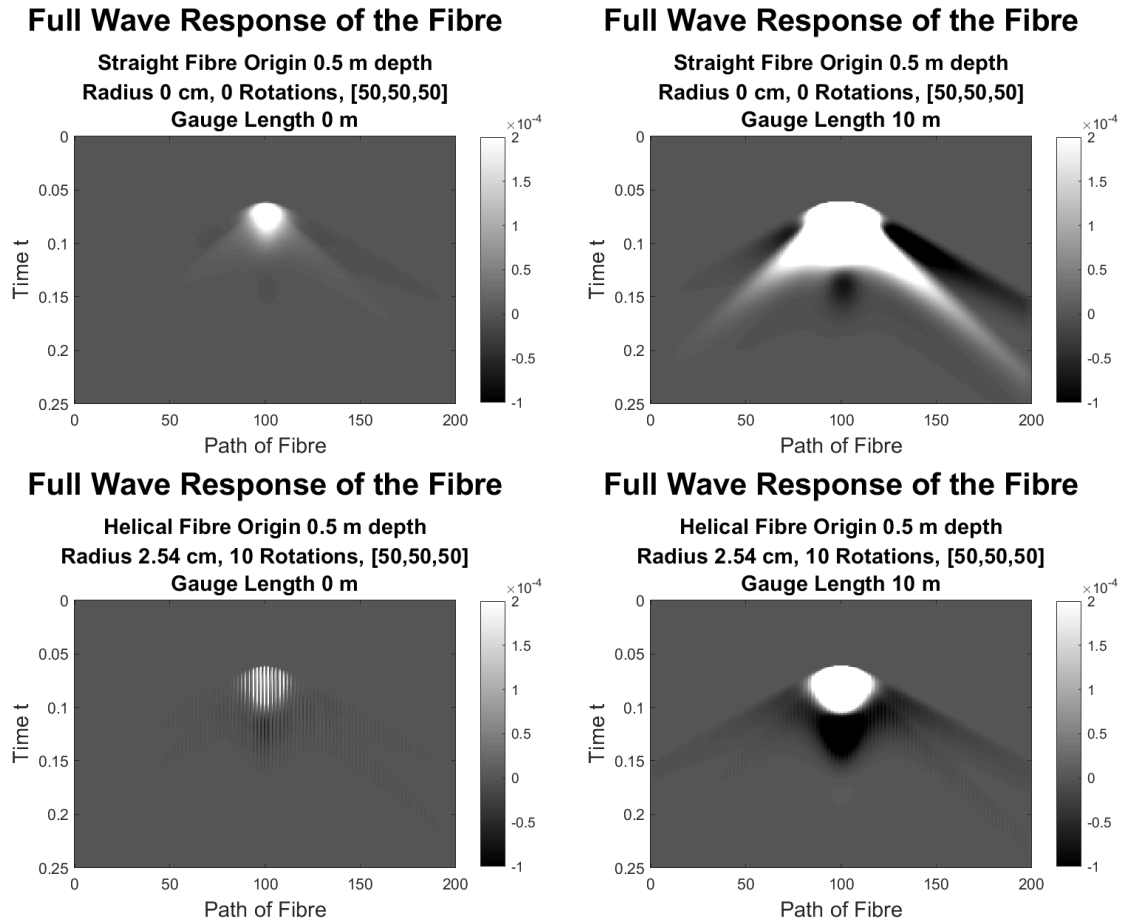


FIG. 10: (Left column) The data without the gauge length applied (top) straight fibre and (bottom) helical fibre at Location 4. (Right column) The 10m gauge length applied to data seen in the left column at Location 4.

Analysis of the data along the deformation

Investigating whether the results increase or decrease over w would provide insight into how the helical fibre compares to the straight fibre. Given that the output of the homotopy model is a matrix for each value of w , we use the L^2 -norm to offer a comparison of each w along the deformation. We first study the L^2 -norm of the data without a gauge length applied and the L^2 -norm of the data with a gauge length of 10m applied. Afterwards, we examine the effects on the trace, determinant, and eigenvalues of the strain matrix at each point $(\mathbf{p}(s), t)$ on the fibre path \mathbf{p} at time t . We use the model from Hardeman-Vooy's and Lamoureux (2018) for this deformation model. The S-wave response is a vector potential which is represented using the S-wave orientation vector \mathbf{A} . To investigate the effect of different S-wave orientations, we also include eight different S-wave orientation vectors to study the effect that the orientation of the S-wave has on the amplitude response of the fibre over the homotopy.

The results above consider a uniform response for the S-wave orientation vector $\mathbf{A} = [50, 50, 50]$. While not included here, we also conducted an experiment where we looked at less uniform values of \mathbf{A} which we group into two sets. The first set of S-wave orientation vectors is $\mathbf{A} = [50, 20, 20]$, $\mathbf{A} = [20, 50, 20]$ and $\mathbf{A} = [20, 20, 50]$. While the data sets are not presented here, we do include information about the data sets in the our following comparisons.

Our first comparison looks at the norm of the data without the gauge length applied. We also include the results of applying the norm to the data when the gauge length is applied. In both cases, we applied the norm at each point w . In Figure 11, we see the results for the vectors $\mathbf{A} = [50, 50, 50]$, $\mathbf{A} = [50, 20, 20]$, $\mathbf{A} = [20, 50, 20]$, and $\mathbf{A} = [20, 20, 50]$ for each of the four locations. Figure 12 shows the norms when the gauge length is applied for these vectors \mathbf{A} .

In Figures 11 and 12, for all S-wave orientation vectors \mathbf{A} when taking the L^2 -norm of the data without the gauge length applied, the response of the helically wound fibre is larger than the response of the straight fibre. Once the gauge length is applied to the data, the norm of the response for the helical fibre is lower than the norm of the response for the straight fibre. Given that Location 4 is 11 meters away from the fibre compared to Locations 1 to 3, the norm of the helical fibre's response appears to decrease more in comparison to the norm of the straight fibre's response for all S-wave orientation vectors \mathbf{A} . Only one case of S-wave orientation vectors \mathbf{A} appear to have a helical response which is larger than the straight fibre's response when the gauge length is applied: the case when $\mathbf{A} = [20, 20, 50]$. This only holds true for the first three locations, and not for Location 4. It suggests there are some formations of fibre where the helical fibre provides a better response than the straight fibre once a gauge length is applied to the data; however, it depends on the orientation of the S-wave response and the location of the source.

With regards to the choice of orientation, the S-wave orientation vectors $\mathbf{A} = [20, 50, 20]$ and $\mathbf{A} = [50, 20, 20]$ vary when no gauge length is applied to the data; however, they appear to give very similar results once the gauge length is applied. This may be attributed to the formation of the fibre with regards to the S-wave orientation vector. The uniform

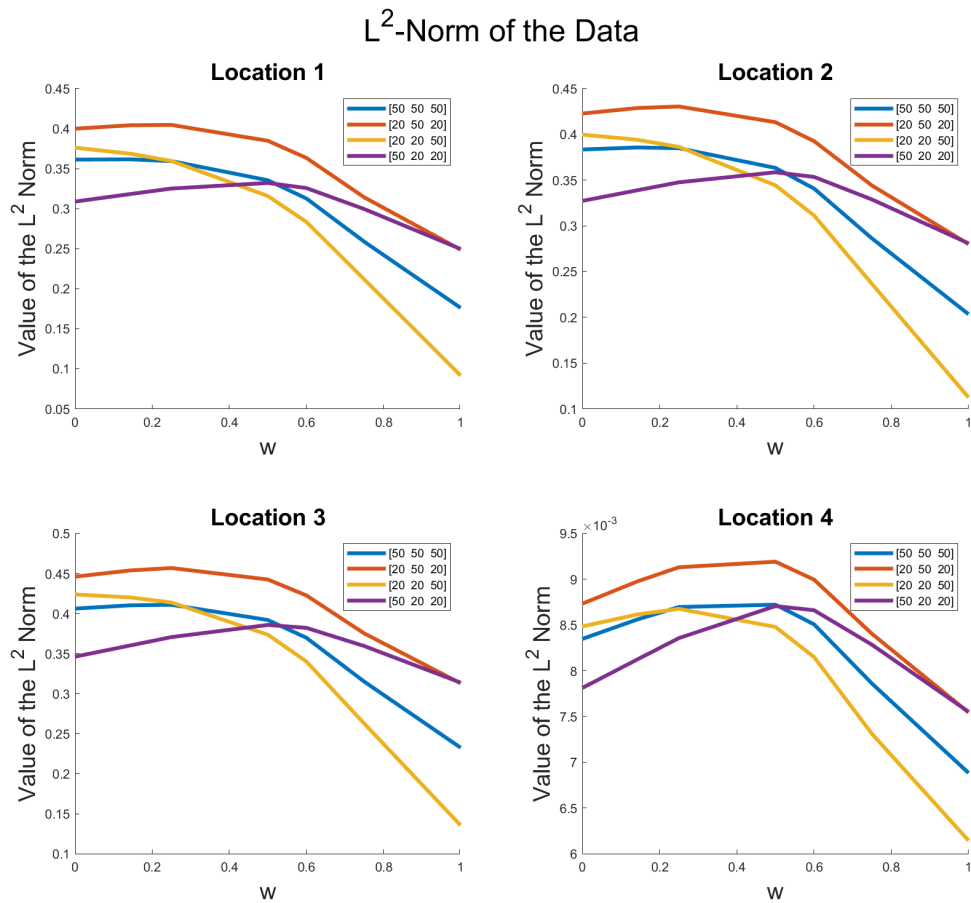


FIG. 11: The L^2 -norm of the data without the gauge length applied at (top left) Location 1, (top right) Location 2, (bottom left) Location 3, and (bottom right) Location 4 for S-wave orientation vectors $\mathbf{A} = [50, 50, 50]$ (blue), $\mathbf{A} = [20, 50, 20]$ (red), $\mathbf{A} = [20, 20, 50]$ (yellow), and $\mathbf{A} = [50, 20, 20]$ (purple).

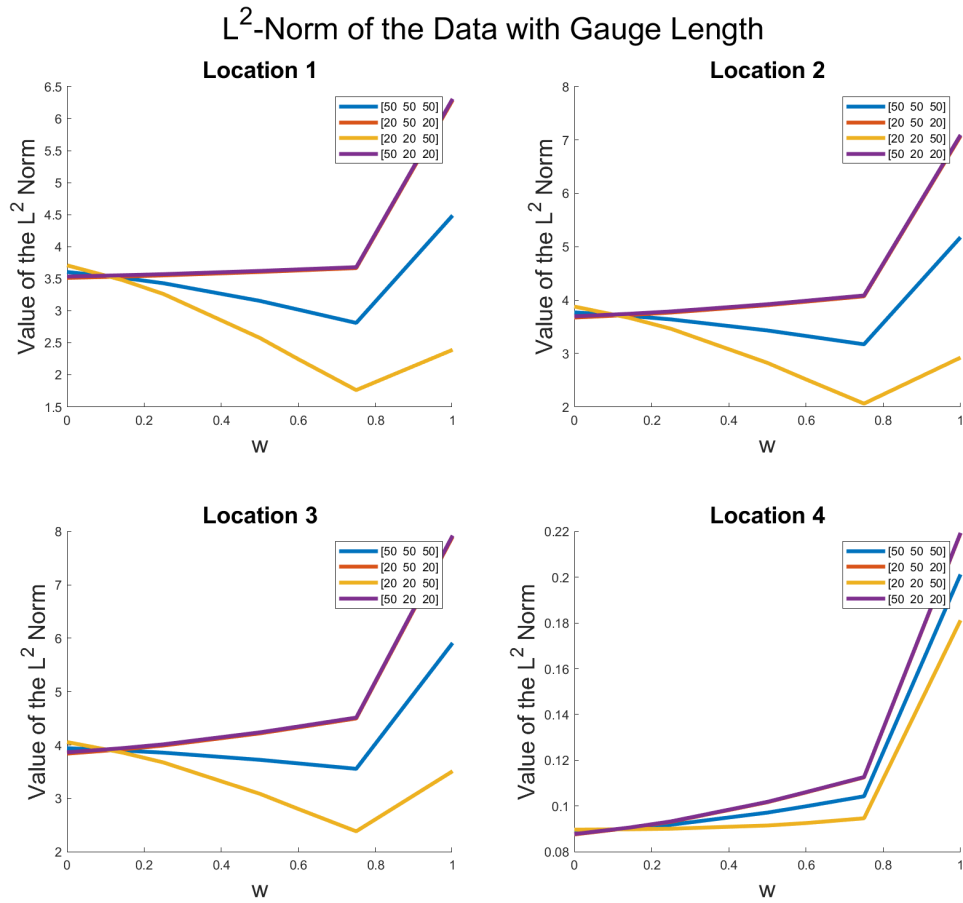


FIG. 12: The L^2 -norm of the data with the gauge length applied at (top left) Location 1, (top right) Location 2, (bottom left) Location 3, and (bottom right) Location 4 for S-wave orientation vectors $\mathbf{A} = [50, 50, 50]$ (blue), $\mathbf{A} = [20, 50, 20]$ (red), $\mathbf{A} = [20, 20, 50]$ (yellow), and $\mathbf{A} = [50, 20, 20]$ (purple).

S-wave orientation vectors $\mathbf{A} = [50, 50, 50]$ give responses which lie between the results of the other S-wave orientation vectors \mathbf{A} when the gauge length is applied to the data and when it is not. Given the different results for each vector \mathbf{A} , it suggests that the success of the fibre depends on the orientation of the source which follows as the amplitude response is linear with respect to the vector \mathbf{A} .

We also observe that for some S-wave orientation vectors \mathbf{A} , the 2.54cm helical radius response ($w = 0$) does not give the largest norm of the data without the gauge length applied across the deformation. It occurs for the S-wave orientation vector $\mathbf{A} = [50, 20, 20]$ in Figure 11. When the gauge length is applied to the data, the norm of the data at $w = 0$ is not the minimum over the homotopy for S-wave orientation vectors $\mathbf{A} = [50, 50, 50]$ and $\mathbf{A} = [20, 20, 50]$ in Locations 1, 2, and 3, whereas for S-wave orientation vectors $\mathbf{A} = [20, 50, 20]$ and $\mathbf{A} = [50, 20, 20]$, it only occurs at Location 1. Given these varying results, it supports the fact that the amplitude of the source affects the success of the fibre formation.

Analysis of the strain matrices: Trace

Now, let us explore the effects on the strain matrix ϵ along the deformation. We begin by calculating the trace of the strain matrix at each point (s, t) and assign it to the corresponding entry of a matrix M_{tr} . Then we take the L^2 -norm of the matrix M_{tr} for each w . From linear algebra, the trace simply sums the diagonal of the strain matrix. The general form of the trace is

$$\text{tr}(\epsilon) = -\left(G_\alpha + \frac{1}{r^2}H_\alpha\right), \quad (33)$$

where α is the velocity of the P-wave. Interestingly, the trace is only dependent on the P-wave which means that the trace does not depend on the orientation of the S-wave response.

Figures 13 show the results of computing the norm on the traces. The trace varies over each location. It does decrease from the helically wound fibre's response to the straight fibre's response; however, it appears to stay unchanged between the different S-wave orientation vectors \mathbf{A} . Given that the trace only depends on the P-wave, it follows that the S-wave orientation vector \mathbf{A} would not affect the trace, since the vector \mathbf{A} shows up only in the S-wave response. The norm of the traces remains unaffected by the amplitude of the source, but it does depend on the location of the source since the value of the norm of the traces changes between each location.

Analysis of the strain matrices: Determinants

Another method of comparison using the deformation involves looking at the determinant of the strain tensor. We calculate the general determinant of the strain tensor to be the following equation:

$$\det(\epsilon) = \frac{1}{8r^6} \left(8G_\alpha^3 A + 4G_\alpha^2 G_\beta B + G_\alpha G_\beta^2 C + 8G_\alpha H_\alpha r^2 + G_\beta^3 D + G_\beta^2 H_\alpha E + 8H_\alpha \right) \quad (34)$$

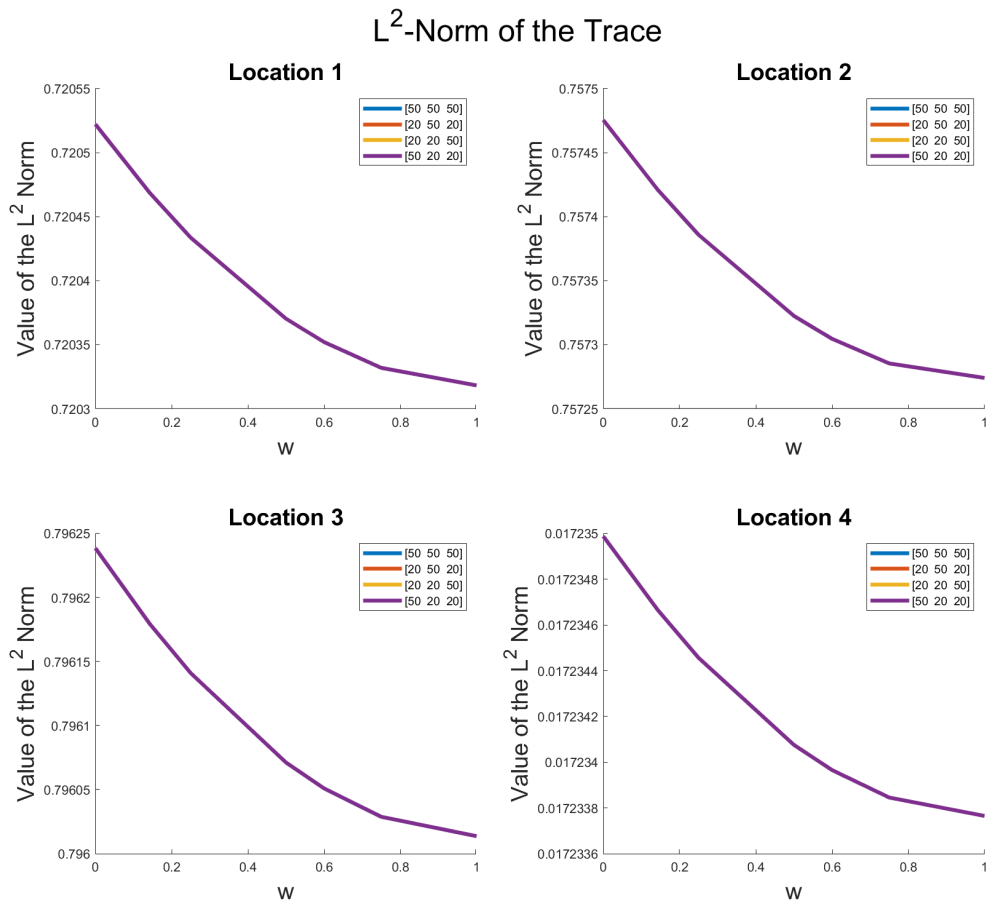


FIG. 13: The L^2 -norm of the traces of the strain matrices of the data at (top left) Location 1, (top right) Location 2, (bottom left) Location 3, and (bottom right) Location 4 for S-wave orientation vectors $\mathbf{A} = [50, 50, 50]$ (blue), $\mathbf{A} = [20, 50, 20]$ (red), $\mathbf{A} = [20, 20, 50]$ (yellow), and $\mathbf{A} = [50, 20, 20]$ (purple).

where

$$A = x^2y^2z(y - z); \quad (35)$$

$$B = -xy\left(2\mathbf{X}yz(z - y) + \mathbf{Y}xz(2z - 3y) + \mathbf{Z}xy(2z - y)\right); \quad (36)$$

$$C = 2\left(\mathbf{X}^2y^3z + \mathbf{Y}^2x^2z(3y - z) - \mathbf{Z}^2x^2y^2\mathbf{X}\mathbf{Y}z(-\mathbf{X}\mathbf{Y}z + 4xy^2 - 3xyz) + \mathbf{X}\mathbf{Z}xy^2(2y - 3z) + \mathbf{Y}\mathbf{Z}x^2y(2y - 3z)\right); \quad (37)$$

$$D = \mathbf{X}\mathbf{Y}(\mathbf{Y}y(\mathbf{X}yz - 2xy) - z^2(\mathbf{X}y + \mathbf{Y}x)) + \mathbf{X}\mathbf{Z}y^2(\mathbf{X}y - (\mathbf{X}z + \mathbf{Z}x)) + \mathbf{Y}\mathbf{Z}x^2(\mathbf{Y}y - (\mathbf{Y}z + \mathbf{Z}y)) + \mathbf{X}\mathbf{Y}\mathbf{Z}y(y - xz) + \mathbf{Y}^3x^2z; \quad (38)$$

$$E = -2\left((\mathbf{X}y - \mathbf{Y}x)^2 + (\mathbf{X}z - \mathbf{Z}x)^2 + (\mathbf{Y}z - \mathbf{Z}y)^2\right) \quad (39)$$

where

$$\mathbf{X} = A_z y - A_y z; \quad (40)$$

$$\mathbf{Y} = A_x z - A_z x; \quad (41)$$

$$\mathbf{Z} = A_y x - A_x y. \quad (42)$$

The functions G and H depend on the minimum-phase source function used. The subscripts on the functions G and H denote whether the P-wave (α) or S-wave (β) velocity is used in the function. The terms \mathbf{X} , \mathbf{Y} , and \mathbf{Z} are the same as the equations found in Hardeman-Vooyoys and Lamoureux (2018).

Given the complicated nature of the equation for the determinant, a numerical comparison of the strain determinants at each point along the fibre would provide more insight at this time. A numerical comparison seems much more feasible since it would be unrealistic to simplify the equation by setting some values of $\mathbf{A}_i = 0$ as the vector \mathbf{A} represents the orientation of the S-wave response. Let us consider the determinant of the strain matrix at each the point (s, t) and take the norm over all (s, t) . Again, we look at the results for all S-wave orientation vectors \mathbf{A} that we studied for the previous comparisons.

As with the trace example, we find the determinant of the strain matrix for each point (s, t) and then assign it to a matrix M_{det} . There will be a matrix M_{det} for each w . We take the L^2 -norm of each M_{det} to generate the Figure 14. Figure 14 shows the L^2 -norm of the determinants for all (s, t) for the first set of S-wave orientation vectors \mathbf{A} at each location. Interestingly, the value of the norm of the determinants does not appear to change over the homotopy for any S-wave orientation vector \mathbf{A} or location; however, they each decrease by a small increment from the helically wound fibre's response to the straight fibre's response. Consistently across all four locations, the S-wave orientation vector $\mathbf{A} = [20, 20, 50]$ provides the highest norms of the determinants out of the four vectors in their group over each location. Both sets of S-wave orientation vectors \mathbf{A} keep the same order from greatest norm to least norm across all four locations.

Analysis of the strain matrices: Eigenvalues

Finally, we compare the eigenvalues of the strain matrices at points (s, t) . Given that ϵ is a 3×3 symmetric matrix, there will be three eigenvalues. From the amplitudes bounds in

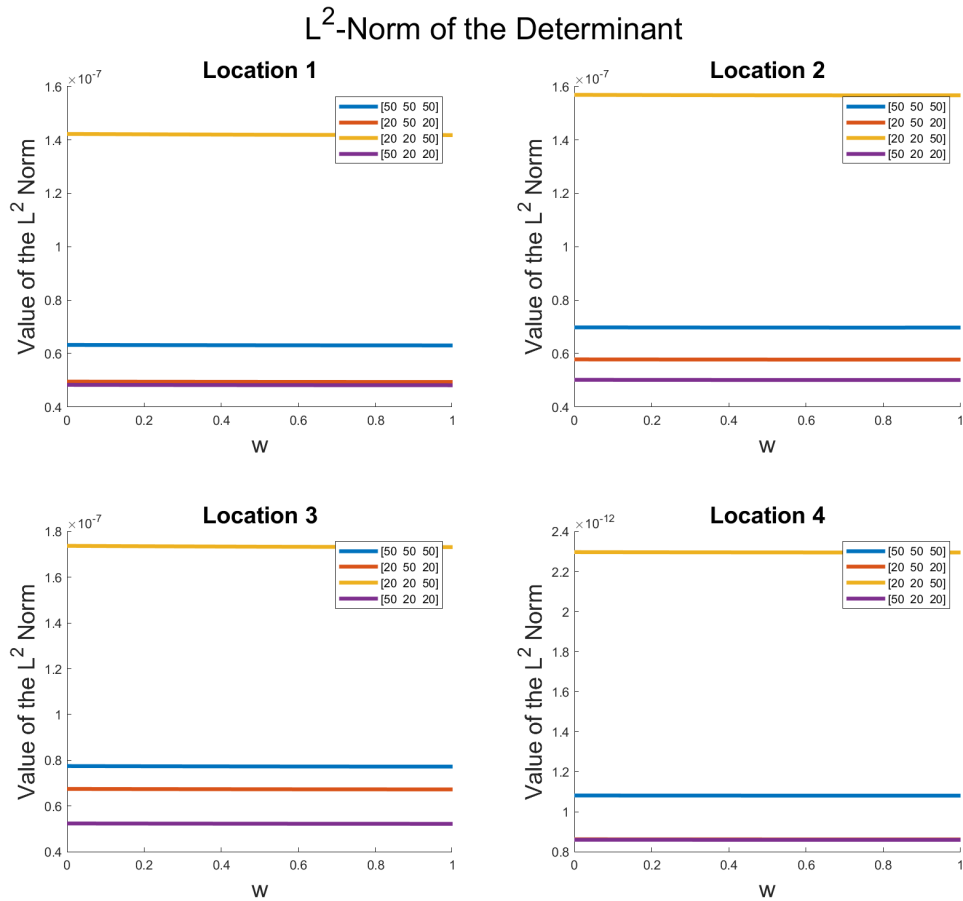


FIG. 14: The L^2 -norm of the determinants of the strain matrices of the data at (top left) Location 1, (top right) Location 2, (bottom left) Location 3, and (bottom right) Location 4 for S-wave orientation vectors $\mathbf{A} = [50, 50, 50]$ (blue), $\mathbf{A} = [20, 50, 20]$ (red), $\mathbf{A} = [20, 20, 50]$ (yellow), and $\mathbf{A} = [50, 20, 20]$ (purple).

Equations 15 and 23, we know that the eigenvalues play an important role with respect to the amplitude of the response. In this section, we calculate the eigenvalues for each strain matrix, group the eigenvalues into three groups, and then compute the L^2 -norm over all (s, t) for three different sets of eigenvalues.

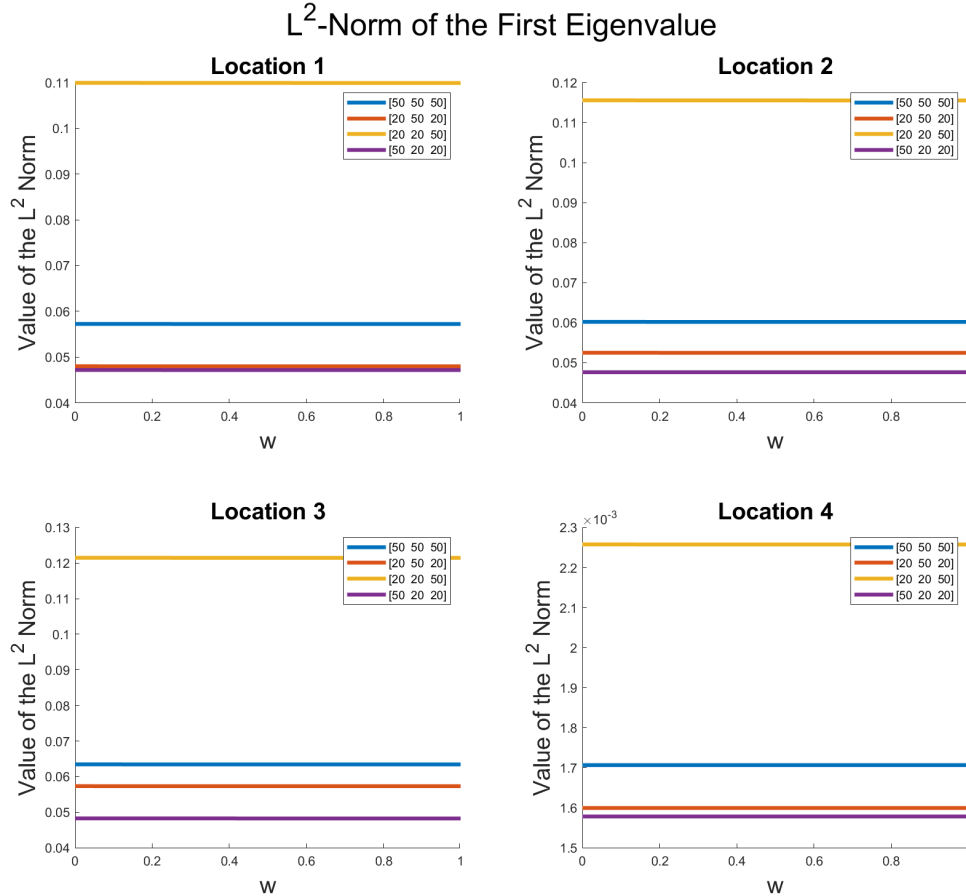


FIG. 15: The L^2 -norm of the first eigenvalues of the strain matrices of the data at (top left) Location 1, (top right) Location 2, (bottom left) Location 3, and (bottom right) Location 4 for S-wave orientation vectors $\mathbf{A} = [50, 50, 50]$ (blue), $\mathbf{A} = [20, 50, 20]$ (red), $\mathbf{A} = [20, 20, 50]$ (yellow), and $\mathbf{A} = [50, 20, 20]$ (purple).

In Figure 15, we see the results of the L^2 -norm applied to the first group of eigenvalues for the S-wave orientation vectors $\mathbf{A} = [50, 50, 50]$, $\mathbf{A} = [20, 50, 20]$, $\mathbf{A} = [20, 20, 50]$, and $\mathbf{A} = [50, 20, 20]$ at each location. As with the norm of the determinants, the first eigenvalues do not appear to change over the deformation. There is a slight change in some of the norms; however, this change is smaller than a factor of 10^{-4} in some cases. As with the case for the norm of the determinants, the S-wave orientation vectors have the same ordering for the norms of the first eigenvalues from greatest to least.

While the L^2 -norms of the second eigenvalues change over each location, Figure 16 shows that the norm stays the same for each S-wave orientation vector \mathbf{A} . Any difference between the norms appears to occur at a factor of 10^{-17} or less which is negligible.

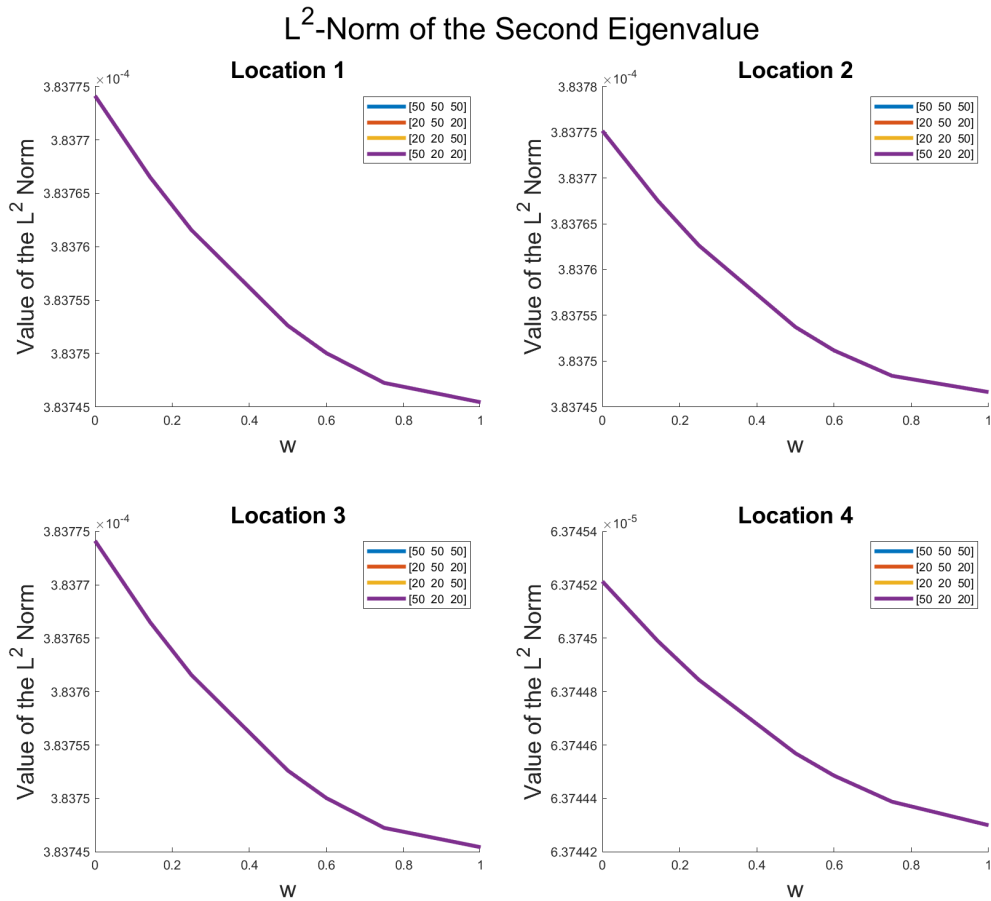


FIG. 16: The L^2 -norm of the second eigenvalues of the strain matrices of the data at (top left) Location 1, (top right) Location 2, (bottom left) Location 3, and (bottom right) Location 4 for S-wave orientation vectors $\mathbf{A} = [50, 50, 50]$ (blue), $\mathbf{A} = [20, 50, 20]$ (red), $\mathbf{A} = [20, 20, 50]$ (yellow), and $\mathbf{A} = [50, 20, 20]$ (purple).

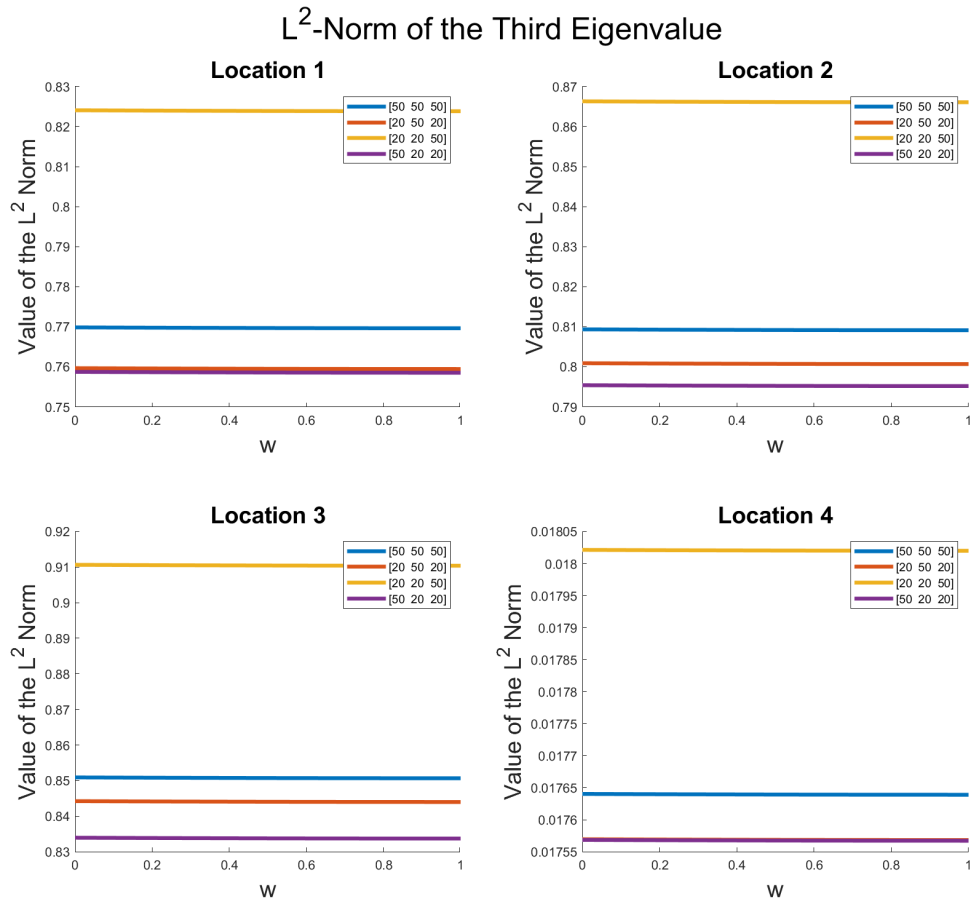


FIG. 17: The L^2 -norm of the third eigenvalues of the strain matrices of the data at (top left) Location 1, (top right) Location 2, (bottom left) Location 3, and (bottom right) Location 4 for S-wave orientation vectors $\mathbf{A} = [50, 50, 50]$ (blue), $\mathbf{A} = [20, 50, 20]$ (red), $\mathbf{A} = [20, 20, 50]$ (yellow), and $\mathbf{A} = [50, 20, 20]$ (purple).

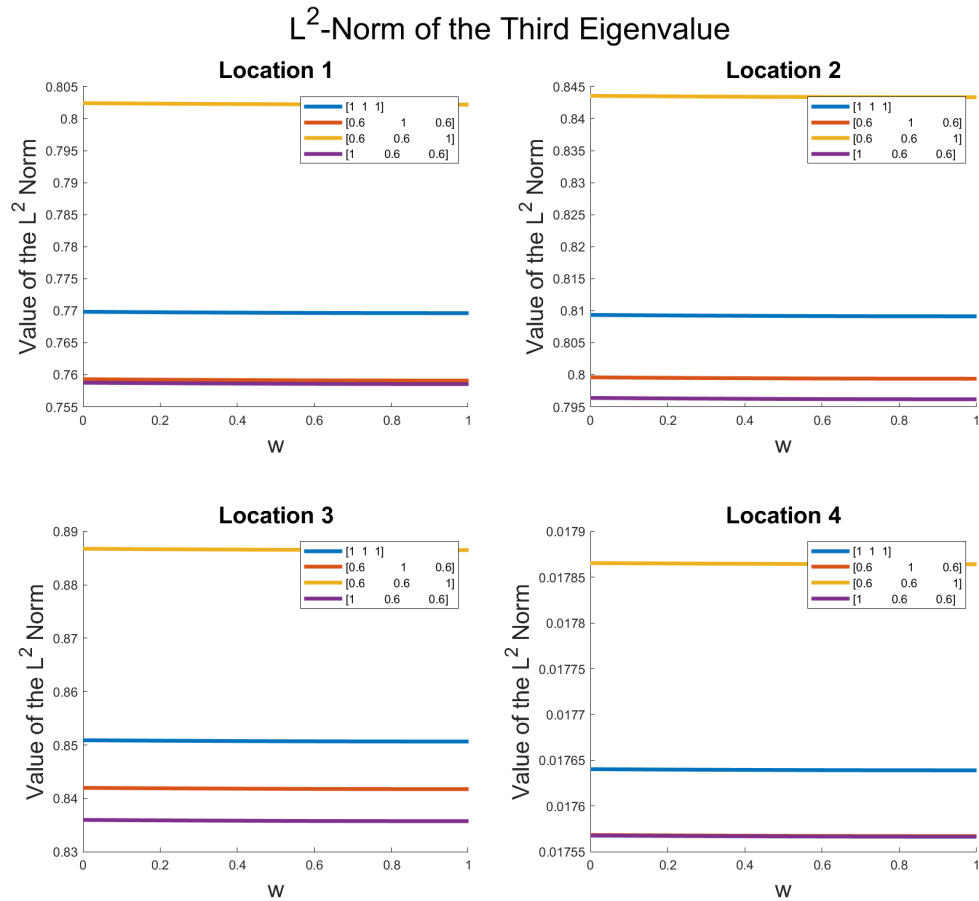


FIG. 18: The L^2 -norm of the third eigenvalues of the strain matrices of the data at (top left) Location 1, (top right) Location 2, (bottom left) Location 3, and (bottom right) Location 4 for S-wave orientation vectors $\mathbf{A} = [1, 1, 1]$ (blue), $\mathbf{A} = [0.6, 1, 0.6]$ (red), $\mathbf{A} = [0.6, 0.6, 1]$ (yellow), and $\mathbf{A} = [1, 0.6, 0.6]$ (purple).

In Figures 17, the L^2 -norm of the third eigenvalues follows a similar pattern to norm of the first eigenvalues; however, the norms of the third eigenvalues are higher at all four locations than the norm of the first eigenvalues. While difficult to detect in the figures, the norm of the third eigenvalues decrease over the deformation from the helically wound fibre to the straight fibre.

FUTURE WORK

With no gauge length applied, helical fibre gives a stronger response than straight fibre. With the gauge length applied, straight fibre gives a stronger response than helically wound fibre. This suggests that the gauge length has a significant effect on the performance of the fibre. In fact, the gauge length appears to destroy a lot of information that the helically wound fibre holds. For this study, we used a gauge length of 10 meters. For future work, an investigation of how smaller and larger gauge lengths affect the helical fibre should be conducted. We should also examine how the gauge length affects the trace, determinants, and eigenvalues of the strain matrices at each point (s, t) .

CONCLUSIONS

Through numerous examples, we demonstrated that with no gauge applied, helical fibre gives a stronger response than straight. With gauge applied, straight fibre gives a stronger response than helical. We also saw that the location of the source with respect to the fibre affects the amplitude response. We found bounds for the amplitude response of the fibre, both when the gauge length is applied and when it is not. We also showed that the amplitude response of the helical fibre is homotopic to the straight fibre by building homotopies between the path of the helical and straight fibres, the strain tensor, and the tangent path of the helical and straight fibres. Then, we used the homotopy for two examples to compare the straight and helical fibre. In the first example, we looked at the results of a helical fibre of radius 2.54cm as it deforms into straight fibre. The norms of the data when the gauge length was applied showed the norm increasing from the helical fibre to the straight fibre along the homotopy; however, for the L^2 -norm of the data when the gauge length was not applied as well as the L^2 -norms of the traces, determinants, and eigenvalues, the L^2 -norm decreased over the homotopy from the helical fibre to the straight fibre.

For deformation comparison of the helical and straight fibre, it is interesting to see that the L^2 -norm of the traces, determinants, and the eigenvalues showed the norms decreasing from helical fibre to the straight fibre. It was only when we applied the gauge length to the data that we saw a difference in the norms. For the horizontal fibre, the norm of the data with the gauge length applied increased from the helical fibre of radius 2.54cm to the straight fibre. These results suggest that the success of the fibre formations is highly dependent on where the source is located with respect to the fibre. Further investigation of the different fibre formations with different locations for the source is merited. Finding other means besides the norm to compare the helical and straight fibre over the deformation is also worth investigating.

ACKNOWLEDGMENTS

We thank the sponsors of CREWES for continued support. This work was funded by CREWES industrial sponsors, and NSERC (Natural Science and Engineering Research Council of Canada) through the grant CRDPJ 461179-13 and the Discovery grant RGPIN-2015-06038 of the third author.

REFERENCES

Hardeman-Vooy's, H. K., and Lamoureux, M. P., 2018, Analytic models of distributed acoustic sensing data for straight and helical fibre: CREWES Research Report, **30**, 1–17.

Rotman, J. J., 1988, *An Introduction to Algebraic Topology*: Springer-Verlag New York Inc.